World Academy of Science, Engineering and Technology
International Journal of Biomedical and Biological Engineering
Vol:5, No:11, 2011

Shape Restoration of the Left Ventricle

May-Ling Tan, Yi Su, Chi-Wan Lim, Liang Zhong, Ru-San Tan

***Abstract*—**This paper describes an automatic algorithm to restore the shape of three-dimensional (3D) left ventricle (LV) models created from magnetic resonance imaging (MRI) data using a geometry-driven optimization approach. Our basic premise is to restore the LV shape such that the LV epicardial surface is smooth after the restoration. A geometrical measure known as the *Minimum Principle Curvature* (κ_2) is used to assess the smoothness of the LV. This measure is used to construct the objective function of a two-step optimization process. The objective of the optimization is to achieve a smooth epicardial shape by iterative in-plane translation of the MRI slices. Quantitatively, this yields a minimum sum in terms of the magnitude of κ_2, when κ_2 is negative. A limited memory quasi-Newton algorithm, L-BFGS-B, is used to solve the optimization problem. We tested our algorithm on an *in vitro* theoretical LV model and 10 *in vivo* patient-specific models which contain significant motion artifacts. The results show that our method is able to automatically restore the shape of LV models back to smoothness without altering the general shape of the model. The magnitudes of in-plane translations are also consistent with existing registration techniques and experimental findings.

***Keywords*—**Magnetic Resonance Imaging, Left Ventricle, Shape Restoration, Principle Curvature, Optimization

I. Introduction

BREATH-HOLD cine Magnetic Resonance Imaging (MRI) is an advanced imaging technique for cardiac morphology and function assessment in clinical practice. While conventional methods of evaluation are based on MRI images, several recent methods [1], [2] have transited to utilize three-dimensional (3D) models reconstructed from the MRI data. However, factors such as respiration and patient movement contribute to misalignments in the MRI data which results in inaccuracies in the 3D models. While MRI scans can be acquired over multiple phases of the cardiac cycle in about 12 seconds to avoid errors induced by respiratory motions, many subjects are not able to hold their breath for prolonged periods. Moreover, MRI data acquired over different breath-hold positions also induce errors in the reconstructed models.

Cardiac image registration methods are often used to compensate for these motions. Existing methods include external skin marker-based techniques [3], landmark-based techniques [4] and thorax surface-based techniques [5]. In [6], the paper reviewed a number of cardiac image registration methods. They are categorized into geometric image feature approach and voxel similarity measure approach. In the first category, registration relies on geometric features such as point-based, surface-based or edge-based registration. In the latter, registration relies on moments (spatial distribution of the mass of the image), principal axis and intensity difference and correlation methods. Recently, some post-processing methods have also been proposed. The method proposed by Elen *et al.* [7] demonstrates the use of constrained optimization of the intensity similarity of intersecting image lines. This proposed correction method is based on the assumption that the similarity of gray values at the intersection lines of different slices is higher when the relative positioning of the slices is correct than when the slices are misaligned. This method corrects relative positions of all long-axis (LA) and short-axis (SA) slices, using only the LA and SA image data and DICOM header information, by optimizing the full 3D translation and rotation of each image slice.

The main dilemma of using an image registration approach to restore the shape of the LV is that errors induced by motion are already embedded in the images. While multi-view image registration techniques could potentially reduce such errors, these methods are essentially using data which contain error for self-correction. In our work, we make use of morphological knowledge of the LV to drive the shape restoration. Instead of using image-based parameters, such as gray values, our LV shape restoration method is based on geometrical consideration. The basic premise is that the LV epicardial surface must be smooth after the restoration and that the general shape of the LV cannot be lost in the process. The *Minimum Principle Curvature* (κ_2) is used as the geometric measure to quantitate the smoothness of the LV surfaces.

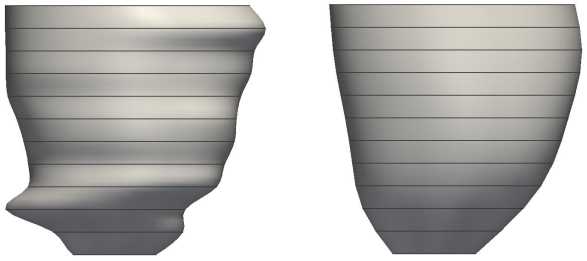

(a) (b)

Fig. 1 Three-dimensional left ventricle mesh models: (a) with motion artifacts, and (b) desired result after shape restoration

The input to our algorithm is an initial 3D LV mesh model reconstructed from contours representing the myocardial borders. Fig. 1 (a) shows a reconstructed 3D LV mesh model from MRI data containing motion artifacts. We aim to achieve a

May-Ling Tan is with the Institute of High Performance Computing, Singapore (phone: 65-6419-1325; fax: 65-6463-1452; e-mail: tanml@ihpc.a-star.edu.sg).

Yi Su is with the Institute of High Performance Computing, Singapore (e-mail: suyi@ihpc.a-star.edu.sg).

Chi-Wan Lim is with the Institute of High Performance Computing, Singapore (e-mail: limcw@ihpc.a-star.edu.sg).

Liang Zhong is with the National Heart Centre, Singapore (e-mail: zhong.liang@nhcs.com.sg).

Ru-San Tan is with the National Heart Centre, Singapore (e-mail: tan.ru.san@nhcs.com.sg).

smooth LV mesh as shown in Fig. 1 (b). This is achieved by shifting the myocardium contours by translating each slice in the in-plane direction. We formulate a smoothness objective function based on κ_2 and solve the problem using a limited memory quasi-Newton optimization algorithm, L-BFGS-B [8]. The L-BFGS-B algorithm is an adaptation of the BFGS algorithm with limited matrix update and it is adept at solving multivariate nonlinear bound constrained optimization problems.

This paper is organized as follows: Section II provides detailed explanation of the methodology of our LV shape restoration algorithm; Section III describes the experiments to test the performance of the algorithm; Section IV discusses the implications of the experimental results and provides direction for future work; and Section V concludes the paper.

II. Method

A. Overview

As the 3D LV models are reconstructed from contours of the myocardial borders, the restoration works by progressively translating these contours in the plane of their respective short-axis (SA) slice. Fig. 2 illustrates the shifting of the contour on a SA slice in the in-plane direction. One can view this as a semi-rigid mesh modification since we are keeping the shape of the contours constant while shifting their position. Without loss of generality, we specify that the SA slices lie parallel to the *xy*-plane. For every slice, a centroid ($X_{C,i}$, $Y_{C,i}$) is calculated by averaging the *x*- and *y*-coordinates of all the points from that particular slice, where *i* is the slice index. The optimization algorithm, L-BFGS-B, will solve for the optimal (X'_C , Y'_C) for all the slices to satisfy a specified objective function representative of the smoothness.

Using the assumption that the LV epicardial surface must be smooth implies a surface with minimum concavity. From a geometry point of view, our objective is to find optimal translations in the *xy*- planes for each individual slice such that the total concavity of the whole LV is at its global minimum. From a computation point of view, we can calculate the minimum principle curvatures κ_2 for every point on the LV epicardial surface mesh to assess the amount of concavity or convexity of the surface. When κ_2 is negative, it implies that the surface at which a point lies on is concaved. Therefore to minimize concavity, the objective function *F* only takes into account the summation of κ_2 values of all points with negative κ_2, that is,

$$F = \sum_{i=1}^{m} \left\{ \| \kappa_{2,i} \| \mid \kappa_{2,i} < 0 \right\} \tag{1}$$

where $\kappa_{2,i}$ is the minimum principal curvature at vertex *i* and *m* is the total number of vertices in the epicardial surface mesh. This will create a balance between concavity and convexity where geometrical kinks will be smoothed out but not at the expense of creating more kinks in other locations. This improves the overall smoothness in the LV shape. Constraints on the translation distance of ($X_{C,i}$, $Y_{C,i}$) are set and the L-BFGS-B algorithm is used to solve the optimal translations in the *xy*-planes of all the SA slices of the LV mesh. The optimal (X'_C , Y'_C) are then used to update the mesh.

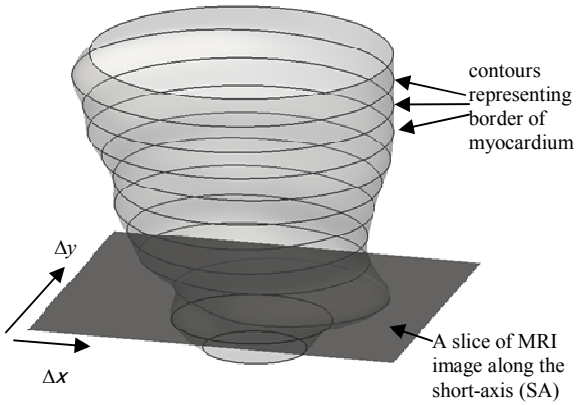

Fig. 2 Modifying shape of 3D LV epicardial surface mesh by translating the contours on SA slice in *x*- and *y*-directions

B. Calculation of Minimum Principle Curvature κ_2

In this section, we discuss briefly the formulation of κ_2. In order to interrogate the geometrical properties of the LV epicardial surface mesh, we use a quadric fitting method to approximate the underlying geometry at every vertex of the mesh. A quadric surface *S* in 3D space can be expressed in the parametric form

$$S(u,v) = \begin{bmatrix} u \\ v \\ au^2 + buv + cv^2 + du + ev \end{bmatrix} \tag{2}$$

where *u* and *v* are the surface parameters and {*a*, *b*, *c*, *d*, *e*} are the quadric coefficients. To fit *S* at a vertex *p*, we select a neighborhood around *p* which represents the region to which *S* is to be fitted. The extent of this neighborhood is quantified by an *n*-ring measure. The quadric coefficients of *S* are then obtained by solving a system of linear equations associated with the *n*-ring neighborhood using a least square method [9].

The surface *S* approximates the local geometry in the vicinity of a point *p* on the 3D mesh model. In differential geometry, the curvature of a surface *S*(*u*,*v*) at a point *p*(*u*,*v*) is evaluated with respect to a normal section. This is done by constructing a plane π such that it passes through the unit surface normal $\hat{n}$ and unit tangent vector in the direction of $\dot{\upsilon}$ (where $\dot{\upsilon} = [\dot{u}, \dot{v}]^T$). The intersection of π with *S* results in a curve called the normal section. The normal curvature $\kappa(\dot{\upsilon})$ can be evaluated by

$$\kappa(\dot{\upsilon}) = \frac{\dot{\upsilon}^T D \dot{\upsilon}}{\dot{\upsilon}^T G \dot{\upsilon}} \tag{3}$$

where $G = \begin{bmatrix} S_u \cdot S_u & S_u \cdot S_v \\ S_u \cdot S_v & S_v \cdot S_v \end{bmatrix} = \begin{bmatrix} E & F \\ F & G \end{bmatrix}$

and $D = \begin{bmatrix} S_{uu} \cdot \hat{n} & S_{uv} \cdot \hat{n} \\ S_{uv} \cdot \hat{n} & S_{vv} \cdot \hat{n} \end{bmatrix} = \begin{bmatrix} L & M \\ M & N \end{bmatrix}$ are the first and second fundamental matrices of the surface, respectively.

The unit surface normal can be calculated by

$$\hat{n} = \frac{S_u \times S_v}{|S_u \times S_v|} \tag{4}$$

In terms of the quadric coefficients, the equation to calculate κ_2 is

$$\kappa_2 = \frac{B \pm \sqrt{B^2 - A^2(4ac - b^2)}}{A^3} \tag{5}$$

where $A = \sqrt{d^2 + e^2 + 1}$ and $B = a + ae^2 + c + cd^2 + bde$. The value of κ_2 is negative when the surface around the point p is concave.

The value of n-ring used in the quadric fitting affects the value of κ_2 because it determines how sensitive the method is to the effect of geometrical variation. With a bigger n-ring value, shape of the surface over a larger extent is interrogated. This takes into account the general variation of the shape, ignoring the high frequency variation in the geometry. With a smaller n-ring value, the shape of the surface over a localized region is inspected. This captures the inter-slice variations in shape.

C. Optimization

As described in the *Overview* section, our goal is to minimize the concavity of the LV epicardial surface. This can be quantified by taking into account the absolute values of κ_2 when it is negative. In mathematical terms, our goal is

$$\min \sum_{\forall \text{ vertices}} \| \kappa_2 \|, \quad \text{where } \kappa_2 < 0 \tag{6}$$

We achieve this by formulating an optimization problem with a suitable objective function, i.e., Eqn. (1). We minimize this non-linear objective function using the L-BFGS-B algorithm [8] which is adept at solving multivariate nonlinear bound constrained optimization problems. It is based on the gradient projection method and uses a limited-memory BFGS matrix to approximate the Hessian of the objective function. The algorithm does not store the results from all iterations but only a user-specified subset. Its advantage is that it makes simple approximations of the Hessian matrices which are still good enough for a fast rate linear convergence and requires minimal storage [8]. This makes it adept at solving large non-linear optimization problems with simple bounds on the variables.

To set up the optimization problem, we can write Eqn. (1) as $F(\mathbf{x})$ with n variables, such that $\mathbf{x}$ contains the centroid coordinates (X_C , Y_C) of the contours on the SA slices, i.e.,

$$\mathbf{x} = \begin{Bmatrix} x_1 & = & X_{C,1} \\ x_2 & = & Y_{C,1} \\ x_3 & = & X_{C,2} \\ x_4 & = & Y_{C,2} \\ \vdots & \vdots & \vdots \\ x_{n-1} & = & X_{C,N} \\ x_n & = & Y_{C,N} \end{Bmatrix}$$

Hence, the number of variables in the optimization problem is twice the number of SA slices, i.e., $n = 2 \times N$. Each of the variables x_i in $F(\mathbf{x})$ is subjected to the bounded-constraints

$$lb_i \le x_i \le ub_i \qquad i = 1, 2, 3, \ldots, n \tag{7}$$

where lb_i and ub_i are the lower and upper bounds of x_i, respectively. In this work, the variables are constrained to translate within a bound of ±20 mm. This value is consistent with what was observed experimentally [10] (expected to be in the range of 0 to 21 mm). The constraint on the translation in the y-direction is

$$-20 \le X'_{C,i} - X_{C,i} \le 20 \tag{8}$$

where $X'_{C,i}$ is the solution and $X_{C,i}$ is the initial x-coordinate of the centroid position of the i-th contour. Similarly, the constraint on the translation in the y-direction is

$$-20 \le Y'_{C,i} - Y_{C,i} \le 20 \tag{9}$$

where $Y'_{C,i}$ is the solution and $Y_{C,i}$ is the initial y-coordinate of the centroid position of the i-th contour.

In addition, the gradient g_i associated with each variable x_i must also be defined such that

$$g_i = \frac{\partial F(x)}{\partial x_i} \tag{10}$$

Since $F(\mathbf{x})$ is in a non-analytical form, we need to approximate g_i using finite differences. In this work, we use the forward difference method to approximate the gradient, i.e.,

$$g_i = \frac{F(x_1, \cdots, x_i + \Delta x_i, \cdots, x_n) - F(x_1, \cdots, x_i, \cdots, x_n)}{\Delta x_i} \tag{11}$$

where Δx_i is a small increment in x_i.

In order to retain the general variation of the LV shape, we perform the optimization in two stages. First, we perform the optimization using an *n*-ring setting of 5 in the computation of the objective function. When *n*-ring = 5, κ_2 is calculated by taking into account points from 5 layers above and below the current SA slice, and 5 points to the right and left of the point of interest. All the slices will shift to minimize the objection function in (1). Next, to further minimize surface concavity over a localized region, the intermediate mesh (updated with the previously obtained solution using *n*-ring = 5) is subjected to a second pass of optimization using *n*-ring = 2. In this case, κ_2 is calculated by taking into account points from 2 layers above and below the current SA slice, and 2 points to the right and left of the point of interest. This second pass is essential to further minimize the concavity over a localized region. The results from setting *n*-ring value = 5 and then *n*-ring = 2 are shown in Fig. 3. As observed, the end result restores smoothness with minimum principle curvature to the LV heart.

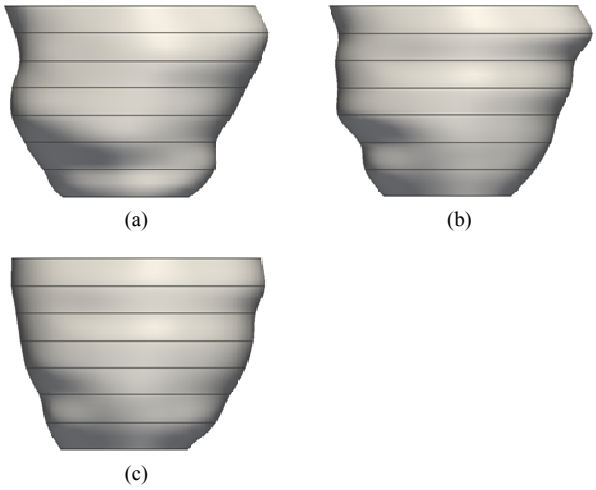

Fig. 3 Shape restoration using two-stage optimization: (a) original mesh with motion artifact, (b) intermediate mesh after optimization using *n*-ring = 5, and (c) final mesh after optimization using *n*-ring = 2

III. Results

A. In vitro Theoretical Model

For theoretical validation of our method, we used an ellipsoidal mesh model for testing. The ellipsoidal model is chosen since it is a widely accepted idealization of the LV chamber. The lengths of the semi-axes are 40 mm, 40 mm and 80 mm. Five contours are randomly chosen and shifted some distance away from their original location in the *x*- and *y*-directions. The limits are set to 11.5mm in the anterior direction, 1.3mm in the posterior direction, 1.8mm to the left and 6.1mm to the right, in accordance to [10]. The theoretical model and the result after a two-stage optimization (i.e., running with *n*-ring = 5 followed by *n*-ring = 2) are shown in Fig. 4. From the figure, we observed that smoothness is restored.

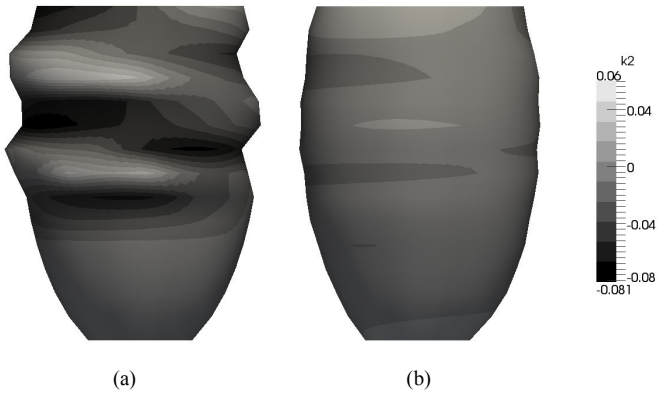

Fig. 4 Theoretical model: (a) with random slice displacement, and (b) after two-stage optimization using *n*-ring = 5 followed by *n*-ring = 2

B. In vivo Patient-specific Models

To further validate the applicability of our method, we tested our algorithm on 10 patient-specific 3D LV models reconstructed from MRI data containing motion artifacts. The MRI scan was performed using breath-held steady-state free precession technique on a 1.5T Siemens scanner (Avanto, Siemens Medical Solutions, Erlangen). TrueFISP (fast imaging with steady-state precession) MR pulse sequence with segmented k-space and retrospective electrocardiographic gating were used to acquire 2D cine images of the LV in the LA plane, as well as a parallel stack of 2D cine images of the LV in the SA plane, from the LV base to apex (8 mm interslice thickness, no interslice gap). Each slice was acquired in a single breath hold, with 25 temporal phases per heart cycle.

The epicardial and endocardial borders of contiguous SA slices were manually delineated by an experienced cardiologist using a commercially-available software CMRtools (Cardiovascular Imaging Solution, UK). Both SA and LA views were utilized to carry out 3D LV reconstruction at the end-diastole phase.

We tested our algorithm with 10 patient samples. Three of the patient samples and their corresponding LV shape restoration results are shown in Fig. 5.

IV. Discussion

A. Results

From the results, we observed that the shape restoration of the LV epicardial surface was successful. Visually, we verified that the asymmetry of the LV geometry was preserved while the geometrical kinks on the surface were significantly reduced. Quantitatively, the absolute values of κ_2 were reduced considerably after the shape restoration, as shown in Fig. 5. The results of the 10 patients indicated that average contour displacements in the *x*- and *y*-directions on the SA planes were 1.62 ± 0.87 mm and 1.46 ± 0.96 mm, respectively. Validation of results of our shape restoration technique with clinical results is important for the method to be accepted clinically. Registration methods are often validated using external

markers or anatomical landmarks [11]. However such validations are difficult because they are not readily available. In our work, we compared the mean contour displacement values of our method with those of existing image registration techniques [6], as shown in Table 1. The minimum and maximum translations in the *x*- and *y*-directions lie between 0 to 4.8 mm, while our results lie in the range of 0.5 to 2.5 mm. Therefore, we conclude that our results are within the range with the existing literature.

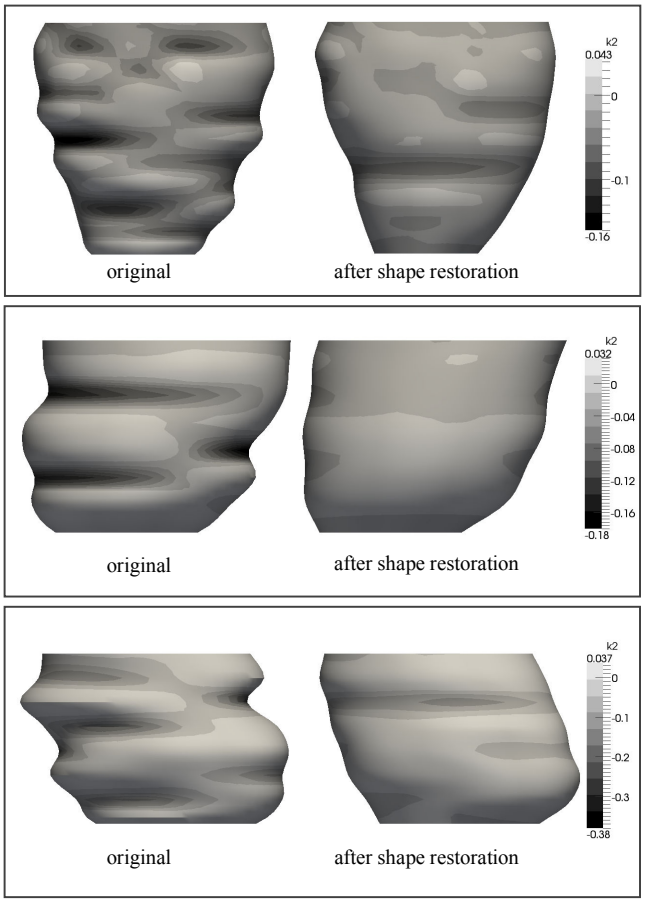

Fig. 5 Three samples of patient-specific 3D LV mesh model before and after two-stage shape restoration

B. Limitations and Future Work

In our current algorithm design, we have only considered translational displacement of the SA slices. However, in actual fact, motion artifacts are also generated by rotational movement, as well as motion in and out of the SA slice planes. In our future work, we will incorporate additional degree of freedoms in the contour movement by including rotation of the SA slices, and motion in a direction orthogonal to the SA slice planes. In addition, the existing form of our algorithm uses a semi-rigid geometrical deformation process to restore the shape of the LV epicardial surface. In future work, we will incorporate free form deformation to the algorithm. We aim to do this by using an error-restricted volume-preserving local smoothing process.

TABLE I
OVERVIEW OF EVALUATED CARDIAC AND THORAX IMAGE REGISTRATION METHODS [6]

Thorax surface based registration	
Reference	Movement Correction (mm)
[12]	2.19 ± 0.52
[13]	(*x*,*y*) 3.0
[14]	2.8 ± 0.5
Heart surface based registration	
Reference	Error (mm)
[15]	2.7
[16]	1.95 ± 1.6
[17]	2.5
Intensity difference and correlation methods	
Reference	Error (mm)
[18]	(*x*)1.23 ± 0.06, (*y*) 3.25 ± 1.04
[19]	(*x*) 3.0, (*y*) 1.6
[20]	(*x*,*y*,*z*) 1.0
[21]	(*x*,*y*) 1.7
[22]	(*x*) 1.9, (*y*) 2.4
[23]	(*x*,*y*) 0.5 ± 0.5
[24]	2.5 ± 1.2
[25]	3.1 ± 1.7
[26]	(*x*,*y*,*z*) 1.5

V. CONCLUSION

In this paper, we presented an automatic algorithm to restore the shape of a 3D LV mesh model using a geometry-driven optimization approach. The method used an analytical surface fitting method to approximate the geometry of the LV mesh and computed the minimum principal curvature as a quantification of the surface smoothness. Next, a limited memory quasi-Newton algorithm, L-BFGS-B, was used to correct the positions of all SA slices to achieve an optimal shape with minimal concavity. To retain the overall shape of the LV mesh, such as its asymmetrical configuration, we performed optimization using *n*-ring = 5. Next, to achieve localized smoothing, we performed a second pass of optimization using *n*-ring = 2. A set of *in vitro* simulated data and 10 *in vivo* LV epicardial datasets at end-diastole are used as inputs to investigate the performance of our shape restoration algorithm. The results showed that there were significant improvements in the smoothness of the LV mesh both visually and quantitatively (in terms of the magnitude of minimum principal curvature). Also, our algorithm was successful in preserving the overall shape of the LV mesh without over smoothing. The mean displacements in the *x*- and *y*- directions are 1.78 ± 1.88 mm and 1.63 ± 2.96 mm, respectively. These values are consistent with results of existing image registration techniques. In future work, we will incorporate additional rotational and through-plane degrees of freedom, as well as free form deformation to enhance the results of the shape restoration.

ACKNOWLEDGMENT

This work was supported by the Science and Engineering Research Council (SERC), Agency for Science, Technology and Research (A*STAR) Singapore through the award of Project Grant 0921480071.

REFERENCES

[1] L. Zhong, Y. Su, L. Gobeawan, S. Sola, R.-S. Tan, J. L. Navia, D. N. Ghista, T. Chua, J. Guccione, and G. S. Kassab, "Impact of surgical ventricular restoration on ventricular shape, wall stress, and function in heart failure patients," *Am. J. Physiol. Heart Circ. Physiol*., 300(5): H1653-H1660, 2011.

[2] L. Zhong, Y. Su, S. Y. Yeo, R.-S. Tan, D. N. Ghista, and G. Kassab, "Left ventricular regional wall curvedness and wall stress assessment in patients with ischemic dilated cardiomyopathy," *Am. J. Physiol. Heart Circ. Physiol*., 296(3): H573-H584, 2009.

[3] Q. Li, L. Zamorano, Z. Jiang, F. Vinas, and F. Diaz, "The application accuracy of the frameless implantable marker system and analysis of related affecting factors," in Lecture Notes in Computer Science 1496: *Medical Image Computing and Computer-Assisted Intervention*, MICCAI98, W. M. Wells, A. Colchester, and S. Delp, Eds., 1998, pp. 253–260.

[4] S. Eberl, I. Kanno, R. R. Fulton, A. Ryan, B. F. Hutton, and M. J. Fulham, "Automated interstudy image registration technique for SPECT and PET," *J. Nucl. Med*., vol. 37, no. 1, pp. 137–145, 1996.

[5] G. J. Klein and R. H. Huesman, "Four-dimensional processing of deformable cardiac PET data," *Med. Image Anal*., vol. 6, pp. 29–46, 2002.

[6] T. Mäkelä, P. Clarysse, O. Sipilä, N. Pauna, Q. C. Pham, T. Katila, and I.E. Magnin, "A review of cardiac image registration methods", *IEEE Transaction on Medical Imaging*, 21, pp. 1011-1021, 2002.

[7] A. Elen, J. Hermans, J. Ganame, D. Loeckx, J. Bogaert, F. Maes, and P. Suetens, "Automatic 3-D breath-hold related motion correction of dynamic multislice MRI", *IEEE Transaction on Medical Imaging*, 29, pp. 868-878, 2010.

[8] C.-Y. Zhu, R. H. Byrd, P.-H. Lu, and J. Nocedal, "L-BFGS-B: Fortran Subroutines for large-scale bound constrained optimization," in *ACM Transactions on Mathematical Software (TOMS)* Vol. 23 Issue 4, Dec. 1997.

[9] Y. Su, L. Zhong, C.-W. Lim, D. Ghista, T. Chua, and R.-S. Tan, "A geometrical approach for evaluating left ventricular remodeling in myocardial infarct patients," *Comput. Methods Programs Biomed*., 2011, in press. DOI:10.1016/j.cmpb.2011.03.008

[10] K. McLeish, D. L. G. Hill, D. Atkinson, J. M. Blackall, and R. Razavi, "A study of the motion and deformation of the heart due to respiration," *IEEE Transaction on Medical Imaging*, 21, pp. 1142-1150, 2002.

[11] R. P Woods, *Handbook of Medical Imaging*: Processing and Analysis. New York: Academic, 2000, ch. Validation of registration accuracy, pp. 491-497.

[12] S. Pallotta, M. C. Gilardi, V. Bettinardi, G. Rizzo, C. Landoni, G. Striano, R. Masi, and F. Fazio, "Application of a surface matching image registration technique to the correlation of cardiac studies in positron emission tomography by transmission images," *Phys. Med. Biol*., vol. 40, pp. 1695–1708, 1995

[13] M. C. Gilardi, G. Rizzo, A. Savi, C. Landoni, V. Bettinardi, C. Rossetti, G. Striano, and F. N. Fazio, "Correlation of SPECT and PET cardiac images by a surface matching registration technique," *Comput. Med. Imag. Graph.*, vol. 22, pp. 391–398, Dec. 1998.

[14] T. J. Mäkelä, P. Clarysse, J. Lötjönen, O. Sipilä, K. Lauerma, H. Hänninen, E.-P Pyökkimies, J. Nenonen, J. Knuuti, T. Katila, and I. E. Magnin, "A new method for the registration of cardiac PET and MR images using deformable model based segmentation of the main thorax structures," in Lecture Notes in Computer Science 2208: *Medical Image Computing and Computer-Assisted Intervention*, MICCAI01, W. J. Niessen and M. Viergever, Eds., 2001, pp. 557–564.

[15] T. L. Faber, R. W. McColl, R. M. Opperman, J. R. Corbett, and R. M. Peshock, "Spatial and temporal registration of cardiac SPECT and MR images: Methods and evaluation," *Radiology*, vol. 179, no. 3, pp. 857–861, 1991.

[16] S. Sinha, U. Sinha, J. Czernin, G. Porenta, and H. R. Schelbert, "Noninvasive assessment of myocardial perfusion and metabolism: Feasibility of registering gated MR and PET images," *Amer. J. Roentgenol.*, vol. 36, pp. 301–307, 1995.

[17] S. Nekolla, T. Ibrahim, T. Balbach, and C. Klein, Understanding Cardiac Imaging Techniques—From Basic Pathology to Image Fusion, Amsterdam, The Netherlands: IOS Press, 2001, vol. 322, ch. *Coregistration and fusion of cardiac magnetic resonance and positron emission tomography studies*, pp. 144–154.

[18] C. M. Gallippi and G. E. Trahey, "Automatic image registration for MR and ultrasound cardiac images," in Lecture Notes in Computer Science 2082*: Information Processing in Medical Imaging*, IPMI01, M. F. Insana and R. M. Leahy, Eds., 2001, pp. 141–147.

[19] L. M. Bidaut and J.-P. Vallee, "Automated registration of dynamic MR images for the quantification of myocardial perfusion," *J. Magn. Res. Imag*., vol. 13, pp. 648–655, 2001.

[20] S. L. Bacharach, M. A. Douglas, R. E. Carson, P. J. Kalkowski, N. M. Freedman, P. Perrone, and R. O. Bonow, "Three-dimensional registration of cardiac positron emission tomography attenution scans," *Comput. Vision, Graph. Image Process*, vol. 34, no. 2, pp. 311–321, 1993.

[21] T. G. Turkington, T. R. DeGrado, M. W. Hanson, and R. E. Coleman, "Alignment of dynamic cardiac PET images for correction of motion," IEEE Trans. Nucl. Sci., vol. 44, pp. 235–242, Apr. 1997.

[22] G. J. Klein and R. H. Huesman, "Four-dimensional processing of deformable cardiac PET data," *Med. Image Anal*., vol. 6, pp. 29–46, 2002.

[23] C. K. Hoh, M. Dahlbom, G. Harris, Y. Choi, R. A. Hawkins, M. E. Philps, and J. Maddahi, "Automated iterative three-dimensional registration of positron emission tomography images," *J. Nucl. Med*., vol. 34, no. 11, pp. 2009–2018, 1993.

[24] D. Dey, P. J. Slomka, L. J. Hahn, and R. Kloiber, "Automatic three-dimensional multimodality registration using radionuclide transmission CT attenuation maps: A phantom study," *J. Nucl. Med*., vol. 40, no. 3, pp. 448–455, 1999.

[25] S. Eberl, I. Kanno, R. R. Fulton, A. Ryan, B. F. Hutton, and M. J. Fulham, "Automated interstudy image registration technique for SPECT and PET," *J. Nucl. Med*., vol. 37, no. 1, pp. 137–145, 1996.

[26] P. J. Slomka, A. H. Gilbert, J. Stephenson, and T. Cradduc, "Automated alignment and sizing of myocardial stress and rest scans to three-dimensional normal templates using an image registration algorithm," *J. Nucl. Med*., vol. 36, pp. 1115–1122, 1995.